Contents

Abstract

1. Belle II and SuperKEKB (SKB) accelerator

In this first chapter we will see a summary of the principal physics measurements on which the Belle II collaboration concentrates its efforts, focusing on the ones which could take particularly advantage from the upgrade of the vertex detector, discussed in this work. We will also go through the structure and the operation of the SuperKEKB accelerator and Belle II detector, to conclude with a short view on the actual state of measurements.

1.1 Physics program of the B-factories

Belle II is a general-purpose spectrometer, committed to making precision measurements of the Standard Model's parameters (SM) and to looking for the physics Beyond the Standard Model (BSM). In particular the experiment studies the Charge-Parity Violation (CPV) in the B mesons system and it also searches for New Physics (NP) evidences in the decays of B and D mesons, in τ leptons and in the dark matter sector (DM), above all hunting for dark photons.

1.1.1 Opened questions in SM

The SM is a physics theory that describe three of the fundamental interactions involving elementary particles, which are strong, weak and electromagnetic interaction (with the exclusion of the gravitational one). It classifies all known particles up to now in 4 main groups: quark, leptons, bosons and Higgs (figure 1.1 on the following page).

Despite its tremendous success achieved over the years, predicting with high precision new particles and mechanisms unknown until that moment, there are many aspects of the Nature, on which it is unable to give answers. Some of them are listed in the following.

- Three generations of quark and leptons are known, but it is not known wheter they should be the only ones and the reasons behind their mass hierarchy.

- Higgs mechanism is able to explain the cause of elementary particles' masses through spontaneous electro-weak symmetry breaking, but it doesn't justify those of neutrinos.

Figure 1.1: Particle classification in the Standard Model

- The SM also predicts other Higgs-like bosons, potentially vector bosons, whose existance would be justified in some SUper-SYmmetry (SUSY) theories or others of New Physics.

- Another opened question is the matter-antimatter asymmetry in the Universe. Even though CP violation is necessary to explain the current state of the universe, the observed quantity is several orders of magnitude less than needed to explain the matter domination over antimatter, which have allowed the evolution of the universe as we know it today.

- The elements of the Cabibbo-Kobayashi-Maskawa (CKM) matrix, which complex phase is at the foundation of CP Violation (CPV) in the quark flavor sector, are diagonal e it could be suggested the existance of a new symmetry, that exists unbroken at high energy (greater than the order of TeV).

All these opened questions encourage the research of new particles and processes that could give reasonable answers.
At the energy frontier, experiments like the Large Hadron Collider (LHC) in Geneve are looking for new particles created from the proton-proton collision with a center mass energy up to 14 TeV.
At luminosity frontier instead, the trace of new particles and mechanisms is searched in precision measurements of suppressed reactions in flavour physics or in the deviations from SM. The discrepancies indeed, could be interpreted as a clue of new physics beyond SM. The last is the Belle II approach.
Moreove new physics models searched in Belle II are those that include more specific flavor couplings, from which indirect seraches can push the new physics scale much higher than the direct search programs.

1.1.2 Belle II Physics channels

In the following we will see the main physics channels of Belle II, focusing on those that would benefit the most from the upgrade of the whole detector and in particular of the vertex detector.

FLAVOR PHYSICS

CP-violating phases in quark sector:

- as we mentioned above, the amount of CP violation in the SM is not enough to explain the difference observed between baryon-antibaryon matter. New clues of CPV could be found studying the discrepancy between B^0 and $\bar{B}_0$ decay rates, so measuring the time-dependent CP violation in penguin transition of b $\rightarrow$ s and b $\rightarrow$ d quarks (such as B $\rightarrow \phi K^0$ and B $\rightarrow \eta' K^0$). In fact this violation is expected to be very small in the SM, so any significant observation of CPV can be interpreted as a signal beyond the SM.
- Also the CP violation in charm mixing, negligible in the SM, could draw attention to new phenomena in the up-type quark sector.
- Another aspect that need to be understood is the large amount of CP violation in the time-integrated rates of charmless hadronic B decays, such as B $\rightarrow K\pi$ and B $\rightarrow K\pi\pi$, observed by other B factories and LHCb.

Conclusive measurements of time-dependent CP violation require a combination of data size and high precision measurement of Δz (reference in paragraph), the distance between the tag and signal in B meson decay vertices. In this respect, the upgrade of the vertex detector could improve a lot the flavor tagging efficiency losses, due to the beam-induced backgrounds, among the others.

Multiple Higgs bosons: Another fundamental channel is the measurement of the Branching Ratio (BR) of B $\rightarrow \tau\nu$, which is particularly sensitive to the charged Higgs boson (in addition to a neutral SM-like Higgs) that in general couples more strongly to heavier particles. But also the BR of the decay B $\rightarrow D^{(*)}\tau\nu$, where BaBar, Belle and LHCb had already reported some anomalies. Moreover extended Higgs mechanism could introduce extra sources of CP violation. We could notice that semi-tauonic decay measurements, rely on efficient and pure tag side B full reconstruction, and so also on the performance of the Vertex Detector.

Flavor Changing Neutral Current (FCNC):

- For this purpose, measurements of time-dependent CP violation in (...), triple product CP violation asmmetrie in B $\rightarrow$ VV decays, and semileptonic decays B $\rightarrow$ V$l\nu$, V= D^*, ρ are the main approaches.
- It is also important measure b $\rightarrow$ s$\nu\bar{\nu}$ transitions (such as...) which belong to a class of decays with large missing energy.
- ???? Moreover it's necessary to improve FCNC measurements of b $\rightarrow$ d, b $\rightarrow$ s, and c $\rightarrow$ u transitions.

Most analyses with missing energy in the final state utilise hadronic or semileptonic B full reconstruction techniques and the performance of these method is most dependent on low momentum track finding and so on the capabilities of the vertex detector as well.

Sources of Lepton Flavor Violation (LFV): LFV in charged lepton decay (at rates of 10^{-8}) is a key prediction in many neutrinos mass generation mechanism and other models of physics BSM. Belle II has an unrivalled sensitivity to τ decays, because of their production in a clean e^+e^- collision background and the large dataset. The experiment analyze τ leptons to search for LF and CP violation and measurement of the electric dipole moment and (g-2) of the τ.

NON FLAVOR PHISICS

Dark Sector: Belle II has a unique sensitivity to dark matter via missing energy decays. Although most research for NP are indirect, there are different model that predict the existance of new particles at the MeV to GeV scale, that couple to the SM via new gauge asymmetries. They also predict a vast range of hidden particles, including dark matter candidates and new gauge bosons.

In these last two areas, τ and dark sectors physics, the aim is to probe forbidden and ultra-rare transition in low-multiplicity final states with as large dataset as possible. This is mostbly rely on trigger efficiency and new trigger strategies, that could take advantage from the upgrade. Many of these processes can only be accesed at Belle II, so it is fundamental increase the perfomance of the detector.

Binding Hadrons: As time goes on, in other B factories and hadron colliders, a large numbers of states not predicted by conventional mesons interpretation are discovered, changing our understanding of QCD in the low-energy regime. For this reason, study of quarkonia is a fundamental purpose for Belle II. In fact new particles can be produce near resonance, achievable by adjusting the machine energy, or by intial state radiation, which effectively provides a continuum of center of mass energies.

CKM matrix: Belle II is also dealing with the measurements of CKM observable, the matrix elements and their phases, with unprecedented precision.

1.1.3 B meson decay vertices

IMPORTANZA DEI VERTICI SECONDARI

1.2 SuperKEKB accelerator

The Belle II sensitivity in the precision measurements that we sift throug in the previous section, is feasible expecially thanks to the extraordinary performance of the SuperKEKB accelerator which host the (almost) hermetic detector. This complex facility is the result of efforts and efficient collaboration between the researches of KEK laboratory and all the international working groups that partecipate(take part, contribute) to the experiment.

1.2.1 The facility

SuperKEKB is an asymmetric e^+e^- collider with a circumference of 3 km, and a center of mass energy peak equal to $\sqrt{s} = 10.58$ GeV, which corresponds to the mass of the $\Upsilon(4S)$ resonance. Compared to its predecessor KEKB (which started its operation in 1998 and concluded in 2010), the current accelerator has allowed to obtain the highest luminosity ever achieved, equal to 4.7×10^{-34} $cm^{-2}s^{-1}$ in July 2022, using a new scheme to accelerate and collide the beams, the so called *nano-beam scheme*(reference). [This was made possible through some improvements and additions in the components of the accelerator itself]. Moreover the new upgrade of the machine, still under study, will also include (provide for) other intervention expecially to cope with higher background level, in view of further increase of the luminosity.

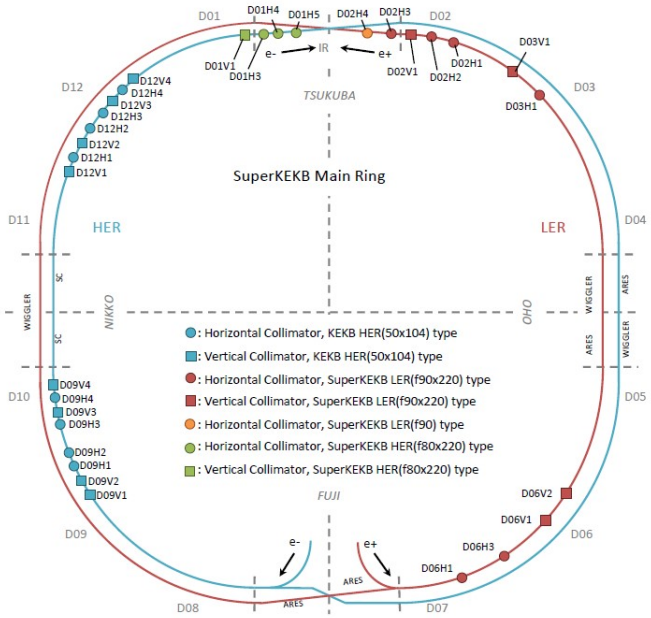

Figure 1.2: SuperKEKB accelerator in 2021. The letters V and H denote respectively vertical and horizontal collimators. Each ring is divided in 12 sections, from the first called D01 to the last D12.

We will briefly see the main features and parameters of the accelerator.

Luminosity

Luminosity is one of the key parameters of an accelerator, it represents the interaction rate per unit of cross section between colliding particles:

$$L = \frac{1}{\sigma}\frac{dN}{dt} \tag{1.1}$$

from which, reversing the equation to obtain N, namely the number of observable physical events:

$$N = \int_0^T L\sigma dt \tag{1.2}$$

where T is the duration of the experiment, σ the cross section of the physical process of interest. (Specifically) In particular luminosity is strictly dependent from machine parameters and from the main characteristics of the beam. With respect to this, it can be expressed as:

$$L = ... \tag{1.3}$$

where .....

As we have already seen, SuperKEKB holds the actual world record in luminosity, with a peak of $4.7 \times 10^{-34}\ cm^{-2}s^{-1}$ with β_y^*= 1.0 mm. In the near future the target will be to reach a luminosity of $6.3 \times 10^{-35}\ cm^{-2}s^{-1}$, increasing current beams and reducing their section in the Interaction Point (IP), squeezing the betatron function up to a value of $\beta_y^* = 0.3$ mm.
For these reasons, the supervision of the beams background becomes one of the most important aspect both to reach the goal and to improve the possible precision measurements of physics.

At present (currently) it is estimated that the background should remain accettable up to a luminosity value equal to $2.8 \times 10^{-35}\ cm^{-2}s^{-1}$ with β_y^*= 0.6 mm. As we shall see, the possibility(hope) to achieve higher luminosity is closely (strictly) relate to an upgrade plan of both the detector and the accelerator.

Beam energy

Energy beams is mostly decided by the physics program interesting for the experiment. Currently SuperKEKB collides an electron beam with energy of 7 GeV (High Energy Ring, HER) , with a positron beam of 4 GeV (Low Energy Ring, LER), reaching a center of mass energy peaked to $\Upsilon(4S)$ resonance.
Also the choice of colliding (using) asymmetric beam (like its predecessor KEKB, which collided (got collide) electrons beam of 8 GeV with a positrons beam of 3.5 GeV) is necessary to identify and measure decay vertices of particles created in the collision (paragraph reference). We have already seen some of the physics behind this choice in section..... [We can notice that the different balance between beam energies (lower beam energy in HER, higher in LER respect to KEKB) was chosen to reduce the beam losses due to Touschek scattering in the LER. This is expected to reduce the spatial separation between B mesons, studied in time-dependent CPV measurements, but leads to slight improvements in solid angle acceptance for missing energy decays].
Indeed this mechanism allows to boost the decay products, improving the ver-

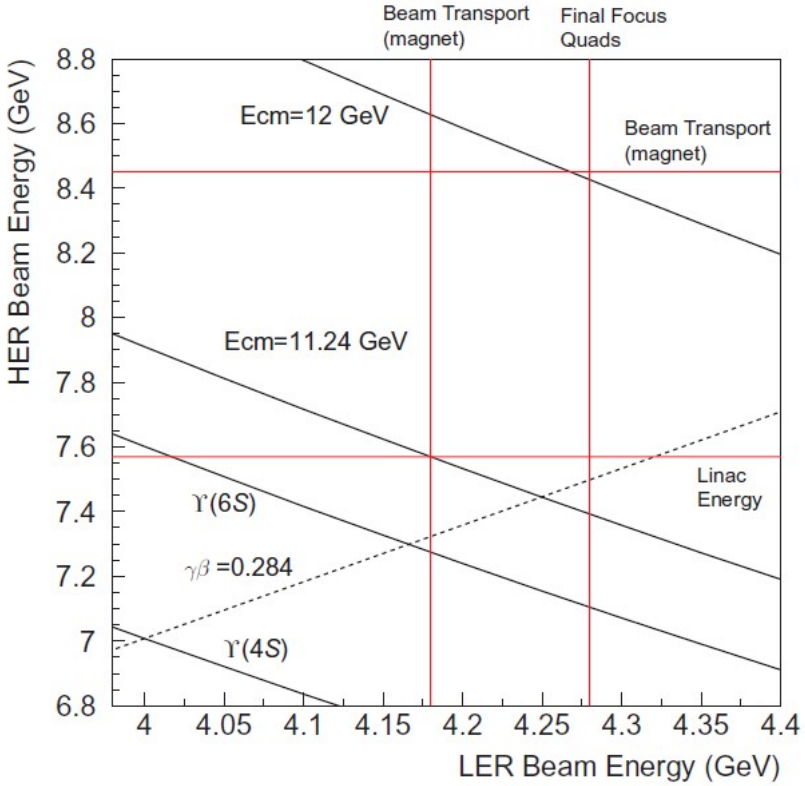

Figure 1.3: Beam energies to reach center of mass energy equal to Υ(4S), Υ(6S), 11.24 GeV and 12 GeV. Horizontal axis represents the energy of LER and the vertical one the energy of HER.

tices reconstruction and increasing the sensitivity of the physics measurement, too. In particular this makes possbile time-dependet measurements, expecially in CP violation.

In figure **??** on page ?? the flexibility of the energy of both beams LER and HER is showed. The possible range covers energies which goes from the Υ(1S) (9.46 GeV) resonance to the Υ(6S) (11.24 GeV), with a peak in 11.24 GeV.

1.2.2 "Nano-beam" scheme

[?]

As mentioned in the previous section, a key element to define the luminosity is the *beta function* β in the Interaction Point (IP). To be able to increase luminosity, it's necessary to decrease the value of β depending on the variation of the other machine parameters, but not only, which are part of its definition (richiama equazione con parametri macchina). The mechanism used in SuperKEKB is called *nano-beam scheme*, and it allowed to obtain luminosity 40 times greater than that of KEKB, managing to (succeding) decrease of 1/20 the β function in the IP.

This new scheme, designed by P. Raimondi, dictates that the beams col-

lide at large angle, in SuperKEKB equal to 83 mrad (keeping beams divided through quadruople magnets), in order to reduce the *hourglass effect*, which succeed when the bunches in the beam are much longer.
We can see briefly the most important parameters that influnce the mechanism?????

The overlap area of the beams is localized and its lenght is given by:

$$d = \frac{\sigma_x^*}{sin\phi_x} \tag{1.4}$$

with ϕ_x defined as half of the crossing angle. The overlap lenght d represent the real lenght of the bunch to consider in the evaluation of the hourglass effect, and it is smaller than the effective bunch lenght along the direction of the beam axis. To reduce this effect, it's necessary to get:

$$\beta_y^* \geq d = \frac{\sigma_x^*}{sin\phi_x} \tag{1.5}$$

Therefore to increase the β function in the IP, the value of d has to diminish, decreasing as aconsequence the horizontal section in the IP and also icreasing the crossing angle. Using a crossing angle large enough, has other positive implications on the operation of the accelerator:

- allows the placement of a new focusing system in the IP with a superconducting quadrupole magnet;
- allows to have two distinct line which host HER and LER beams;
- diminisches the *fringe fields* effect in the IP, wihch are the residuals of the magnets (magnetic fields) in the proximity (nearby).

In figure 1.4 on the facing page are reported the main machine parameters (default value) of the SUperKEKB accelerator.

	LER	HER	Unit
E	4.000	7.007	GeV
I	3.6	2.6	A
N_b	2500		
C	3016.315		m
ε_x	3.2	4.6	nm
ε_y	8.64	11.5	pm
β_x^*	32	25	mm
β_y^*	270	300	μm
$2\phi_x$	83		mrad
α_p	3.25×10^{-4}	4.55×10^{-4}	
σ_δ	8.08×10^{-4}	6.37×10^{-4}	
V_c	9.4	15.0	MV
σ_z	6	5	mm
ν_s	−0.0247	−0.0280	
ν_x	44.53	45.53	
ν_y	44.57	43.57	
U_0	1.87	2.43	MeV
τ_x/τ_s	43.1/21.6	58.0/29.0	msec
ξ_x	0.0028	0.0012	
ξ_y	0.0881	0.0807	
L	8×10^{35}		$\mathrm{cm}^{-2}\,\mathrm{s}^{-1}$

Figure 1.4: Machine parameters of SuperKEKB. The mark "*" indicate values in the IP.

1.3 Belle II detector

Belle II detector is a general-purpose spectrometers, optimized in precision measurements of B mesons and their decay products. Compared to its predecessor Belle, it have to preserve (mantain) good performance despite having smaller boost in the center of mass and suffering greater levels of backgrounds and so of radiations, which are one of the main causes of premature degradation of performance and expected mean life of the detector itself.

Belle II consists of a series of nested subdetectors, which surrounds the IP of the two beams, placed around the berillium beam pipe of 1 cm(10 mm??) of radius. Now we will go trough a briefly description of the several subdetectors.

1.3.1 Vertex Detector (VXD)

The **VerteX Detector (VXD)** is composed by two devices, the silicon Pixel Detector (PXD) and the Silicon Vertex Detector (SVD), for a total of six layers around the beam pipe. PXD('s) two first layers (at a radius of 14 mm and 22 mm, respectively) consist of pixelated sensors of the DEPFET type. The remaining four layers of SVD instead, are equipped with double-sided silicon strip sensors (at 39 mm, 80 mm, 104 mm and 135 mm respectively).

1.3.2 Central Drift Chamber (CDC)

It is the central tracking device, with a large-volume drift chamber and small drift cells. The chamber gas is comprised of a $He-C_2H_6$ 50:50 mixture with an average drift velocity of 3.3 μs^{-1} and a miximum drift time of about 350 ns for a 17 mm cell size. The CDC contains 14336 wires rranged in 56 layers either in *axial* orientation (so aligned with the solenoidal magnetic field) or *stereo* (skewed with respect to the axial wires). In fact by combining information from both the axial and the stereo layers it is possible to reconstruct a full three-dimensional helix track.

1.3.3 Particle identification system (TOP e ARICH)

TOP is a special kind of Cherenkov detector where the two-dimensional information of a Cherenkov ring image is given by the time of arrival and impact position of Cherenkov photons at the photodetector at one end of a 2.6 m quartz bar. It is composed by 16 detector module and each one (of them) consists of a 45 cm wide and 2 cm thick quartz bar with a small expansion volume (about 10 cm long) at the sensor of the bar. At the exit window of the wedge, two rows of sixteen fast multi-anode photon detectors are mounted. This detector requires microchannel plate (MCP) photomultiplier tubes (PMT) specially dveloped for this purpose.

ARICH is used to identify charged particle and it is placed in the forward endcap region. It is a proximity focusing Cherenkov ring imagine detector with aerogel as Cherenkov radiator. The number of detected Cherenkov photons is a key parameter of the RICH and in this experiment it is increased by a novel method. Two 2 cm-thock layers of aerogel with different refractive indices (n =

1.045 upstream, n= 1.055 downstream) are used to increase the yield without degrading the Cherenkov angle resolution. As the single-photon-sensitive high-granularoty sensor, a hybrid avalanche photon detector (HAPD) is used.

1.3.4 Electromagnetic calorimeter (ECL)

The **ECL** is a highly segmented array of tallium-doped caesium iodide CsI(Tl) crystals assembled in a (projective geometry). THis detector is used to detect gamma rays and to identify electrons, and in particular to separate electrons from hadrons (expecially pions). All three detector regions (barrel, forward and backward endcaps) are instrumented with a total of 8736 crystal, covering about 90 % of the solid angle in center-of-mass system.

1.3.5 K_L muon detector (KLM)

It consists of an alternating sandwich of 4.7 cm-thick iron plates and active detector elements located outside the superconducting solenoid. The iron plates serve as the magnetic flux return joke for the solenoid. They also provide 3.9 interaction lenghts or more of material, beyond the 0.8 interaction lenghts of the calorimeter, in chich K_L^0 mesons can shower hadronically. The active detector elements have been chosen in order to cope with the reduction of the detector efficiency under the SuperKEKB background rates. Layers of scintillator strips with wavelenght-shifting fibers are used, the readout instead relies on silicon photomultipliers (SiPMs, Geiger mode operated APDs(...)) as light sensors.

1.3.6 Trigger system

The trigger system of Belle II has a non-trivial role to identify eventsof interest during data-taking. It must work efficiently in the presence of high background rates, while respecting (satisfying) the limitations of the DAQ (?). This system is composed of two levels: a hardware-based low-level trigger (L1) and a software-based high-level trigger (HLT).

- **L1**: has a latency of 5 μs and a maximum trigger output rate of 30 kHz, limited by the read-in rate of the DAQ.
- **HLT**: is a key component of the DAQ and it has to reduce online event rates to 10 kHz for offline storage, and it must identify track regions of interest for PXD readout in order to reduce data flux. It reconstructs events with offline reconstruction algorithms, using all detectors infromation except for the PXD.

1.4 Current state and perspectives of data taking

2. Belle II Upgrade

In this chapter we want to present (expose, introduce) the main reasons in favor of the upgrade of Belle II and in particular of its vertex detector. We will go through the primary sources of background in the experiment and other aspects that make the upgrade necessary. Eventually we will also introduce some of the proposes made for the vertex detector, which is the focus of this thesis.

2.1 Background sources and limits in Belle II (limits, limitations)??

SuperKEKB is already the world's highest-luminosity collider and it aims to reach a new peaks luminosity [of 6.3 10^{35} $cm^{-2}s^{-1}$] in the future by further increasing the beam-currents and reducing the beam-size at the interaction point by squeezing the betatron function down to $\beta_y^* = 0.3$ mm (mentioned in section REFERENCE). For this reason, it's necessary to understand how to mitigate the beam backgrounds where possible and how to cope with the consequent challenges.

In order to estimate the future machine scearios, several simulations and measurements of beam background have be done. This is necessary to study the vulnerability of the subdetectors (and more generally of the machine) and so to design the countermeasures to adopt (against the deterioration of performance and material).

2.1.1 Beam-induced background sources

Here we want to give an overview of the main beam background sources at SuperKEKB.

[We include also luminosity-dependent background such as radiative Bhabha scattering and production of two-photon events.]

Touschek effect : It is an intra-bunches scattering process, where the Coulomb scattering of two particles in the same beam bunch changes the particles' energies, increasing the value of one and lowering(decreasing) that of the other respect to the nominal value. This process(effect) is the first beam background source (at SuperKEKB).

Beam-gas scattering : this represents the scattering of beam particles by residual gas molecules in the beam pipe. It's the second beam background source and it can occur via two processes: Coulomb interactions, which

changes the direction of the beam particle, and bremsstrahlung scattering, which decreases the energy of the beam particles.

These two processes lead to the scattered particle to falling out the stable orbit and to hitting the beam pipe while they propagate around the ring. This cause EM shower that could reach the detector if the loss position is close to it.

Radiative Bhabha scattering and two-photon processes : There are several undesirable collision processes at IP, which have very high cross sections but only little interest for the physics under study in the experiment. Two of them are **Bhabha scattering** ($e^+e^- \to e^+e^-\lambda$) and **Two-photon processes** ($e^+e^- \to e^+e^-e^+e^-$). The photon produced in the first, interacts with the iron magnets and produce a very large amounts of neutrons via the photo-nuclear resonance mechanism. [Such neutrons are the main background source for the outermost Belle II detector, the K_L and muon detector (KLM).] The electrons-positrons pairs of the latter instead, can spiral around the solenoid field lines and leave multiple hits in hte inner Belle II detectors.

These processes increase the Belle II occupancy and radiation dose, and they are reffered as *Luminosity background*. In fact the rate of this type background is proportional to the luminosity. [The future further increasing of luminosity in the experiment, makes the upgrade necessary to deal with with this problem.]

Synchrotron Radiation (SR) : X-rays emitted from the beam, when electrons and positrons pass through the strong magnetic field near the IP. The HER beam is the main source of this type of background, because SR power is proportional to the beam energy squared and magnetic field squared. SR can potentially dammage the inner layers of the vertex detector. [...]

There are also other sources of background beyond those mentioned and during the last decade a well-structured set of countermeasures have been developed, to suppresse (mitigate) each of them.

2.1.2 Current background status and future implications (predictions)

[So it is a of a great importance simulate and measure the background to check on the state of the detector and the machine but also to predict how the conditions could change.] In figure .... the Belle II background level measured in..... is shown. Current background rates in the experiment are acceptable and above all in most cases well below the limits (listed??).

As we have already seen in the previous (ref?) SR is the main background source which could damage(deteriorate) the vertex dector.Event though, the current level is of no concern in terms of occupancy for the innermost layers of the vertex detector, in the case of a large increase, SR may cause inhomogenities in PXD module irradiation, which would make it more difficult to compensate by adjusting the operation voltages of the affected modules.

Until now it can be said that SuperKEKB and Belle II are operating stably. Beam-induced backgorund rates are well below the limits of the detector and do not prevent from increasing further tha current and hence the luminosity (at the same time). But altough background levels are now under control, there are several other difficulties that can limit beam currents and so the possibility to move the luminosity frontier at towards higher levels, allowing Belle II reaserchers to study rare physics processes.

The aim of the experiment is to reach an integrated luminosity of the order of 50 ab^{-1} by 2030. In order to achieve this goal, the upgrades of the experiment togheter with several machine operation schemes, instability and background conutermeasures must be considered and studied (??).

2.2 Purposes of the upgrade

We have seen that SuperKEKB is expected to be able to reach.... with the existing accelerator complex, but in order to achieve higher luminosity, an upgrade (enhancement) of the interaction region will (probably) be required.
Belle II is also designed to operate efficiently under the high levels of backgrounds extrapolated to target luminosity, but safety margins are not large. Moreover in the case of a redesign of the interaction region large uncertainties in the background extrapolations are unavoidable.
The upgrade program is therefore motivated by many considerations:

- Improve detector robustness against backgrounds
- Increase longer termsubdetector radiation resistance
- Provide large safety factors for running at higher luminosity
- Develop the technology to cope with different future papths, for instance if a major IR redesign is required to reach the target luminosity
- Improve overall physics performance

The Belle II upgrade aims to ensure that the detector could have high impact results in heavy flavour and dark sector physics, at the higher level of luminosity ever achieved. The luminosity dependent background conditions may be severe, in terms of detector operations and physics performance. Moreover the current detector configuration is not expected to maintain its performance level when facing high beam background level or high rates.

In regards to the Vertex Detector (in particular), all proposed upgrades aim to:

- reduce occupancy level by employing fully pixelated and fast detector (nowadays CMOS technologies most probably choice)
- increase robustness against tracking efficiency and resolution losses from beam background (better handling of background)
- this implies improved tracking efficiency with $p_T <$ 200 MeV/c.

2.3 Summary of possible vertex detector upgrade

2.3.1 DEPFET

2.3.2 Thin sensor

2.3.3 CMOS MAPS

2.3.4 SOI

3. Il rivelatore VTX

3.1 Layout del rivelatore VTX

3.1.1 iVTX

3.1.2 oVTX

3.2 Simulazioni di performance

3.3 Caratteristiche chip sensore

3.4 Struttura meccanica

4. Sensori CMOS MAPS

4.1 Rivelatori a semiconduttore

4.2 Sensori a pixel monolitici/ibridi

4.3 Tecnologia CMOS MAPS

4.4 Storia degli sviluppi di Monopix

5. TJ-Monopix 2 characterization ??

5.1 Matrix and flavors

5.1.1 Mask (operation) and noisy pixels

5.1.2 Analog and digital readout

5.1.2.1 BCID reset

5.1.2.2 Main registers (and conversion?)

5.1.3 Comparison between data and simulation

In the interest of understanding how the settings of the chip influence the threshold's value, several measurements have been taken varying the values of the main registers which are responsible for it. The results are compared with simulations done by Hung Pham (...). [???]

5.1.3.1 I_{CASN}

This current is responsible of the output baseline. In a few words, higher this value, higher the baseline, lower the threshold and also a little bit the gain.

In figure 5.1, we can see the simulated behaviour of the threshold and the gain, increasing the value o I_{CASN}.

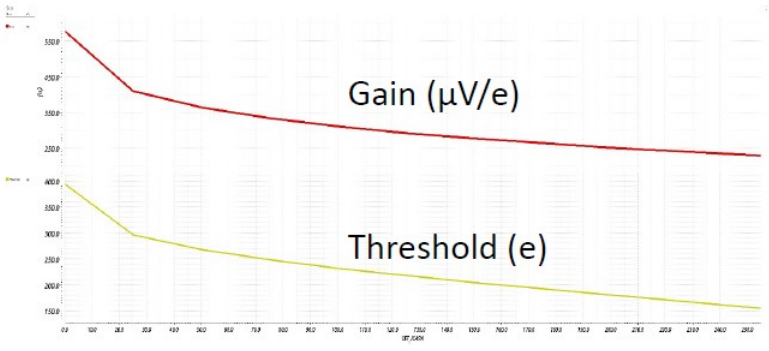

Figure 5.1: Trends of Gain and Threshold increasing I_{CASN}.

To verify the trend of threshold in particular, three different acquisition have been taken by fixing $I_{THR} = 20$, 40, 64 and increasing I_{CASN} from 0 to 30 DAC,

with a step of 5 DAC. We have done this enabling 200 pixels in the Cascode FE (rows: 472 - 512, cols: 225 - 230).[??]

The threshold distributions have been fitted with a gaussian function for each measurement, in order to obtain the average values and their dispersion.

$I_{THR} = 64$:

I_{CASN} [DAC]	THR [DAC]	THR Dispersion [DAC]
0	61.43	2.45
5	53.42	2.45
10	50.33	2.45
15	48.21	2.41
20	46.70	2.38
25	45.49	2.52
30	46.09	2.50

$I_{THR} = 40$:

I_{CASN} [DAC]	THR [DAC]	THR Dispersion [DAC]
0	47.28	2.12
5	41.07	2.02
10	38.39	2.03
15	36.65	1.95
20	35.53	1.91
25	NaN	NaN
30	33.37	2.04

[Here we can see a particular setting, that is $I_{THR} = 40$ AND I_{CASN}=25, for which the chip doesn't seem to work. PIXEL THAT FIRE UP??]

$I_{THR} = 20$:

I_{CASN} [DAC]	THR [DAC]	THR Dispersion [DAC]
0	34.43	1.95
5	28.10	1.72
10	26.59	1.75
15	24.66	1.77

In figure 5.2 on the following page all trends obtained from these data are reported.

[TREND OF DISPERSION?]

5.1.3.2 I_{THR}

Reusing the same data of the previous measurements, the trend of the threshold have been studied, changing the value of I_{THR} and fixing that of I_{CASN}. In this case only I_{CASN} from 0 to 15 DAC is considered, because for higher values we don't have enough measures of the threshold (specifically only two for I_{THR}=40, 64). The results are shown in figure 5.3 on the next page.

We can compare them with the simulation done by Hung Pham in figure 5.4 on page 27.

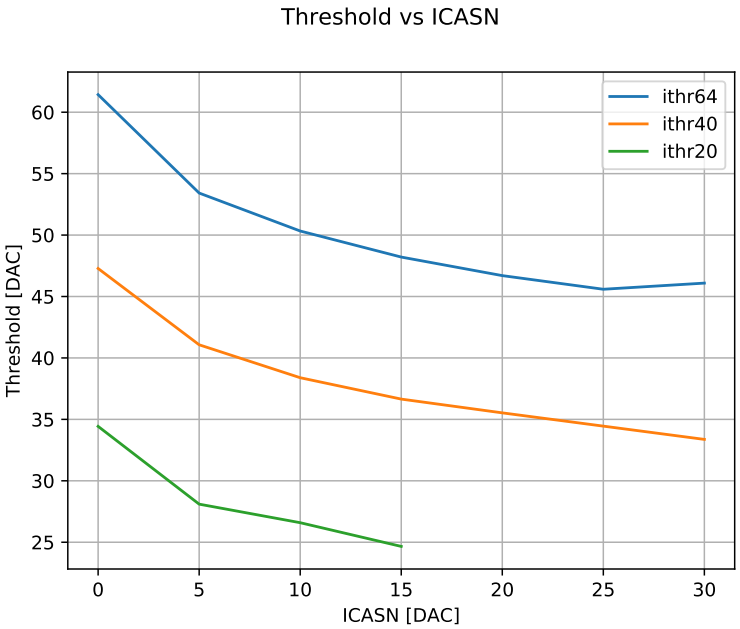

Figure 5.2: Threshold vs. I_{CASN} for I_{THR}= 20, 40, 64.

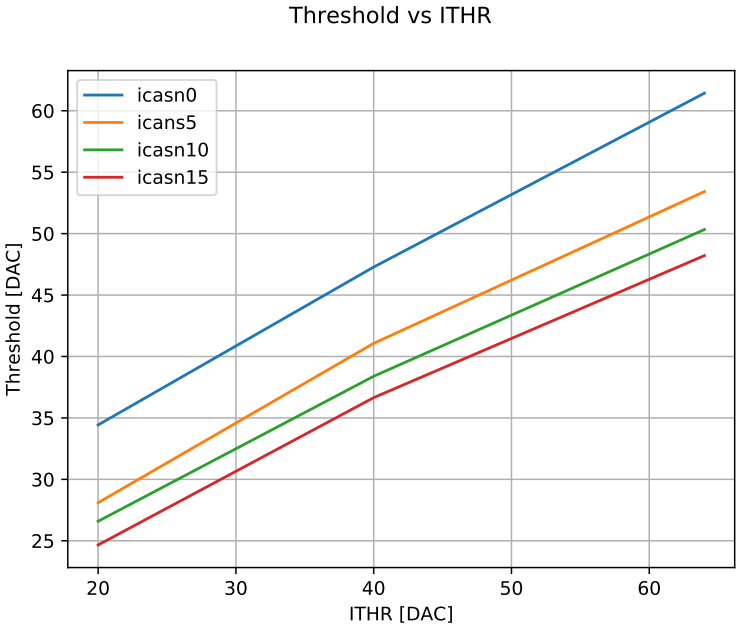

Figure 5.3: Threshold vs. I_{THR} for I_{CASN}= 0, 5, 10, 15.

5.1.3.3 V_{CASP}

[Explain VCASP]

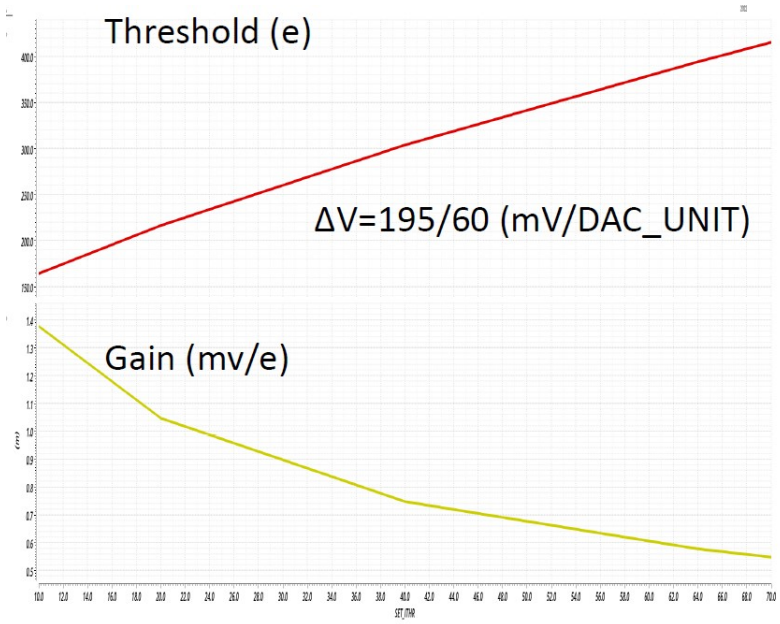

Figure 5.4: Trends of Gain and Threshold increasing I_{CASN}.

In order to enhance this type of analysis, other scans have been run increasing the value of V_{CASP} from 3 to 143, with a step of 10 DAC unit. In figure 5.5 the threshold's trend with respect to different values of this register.

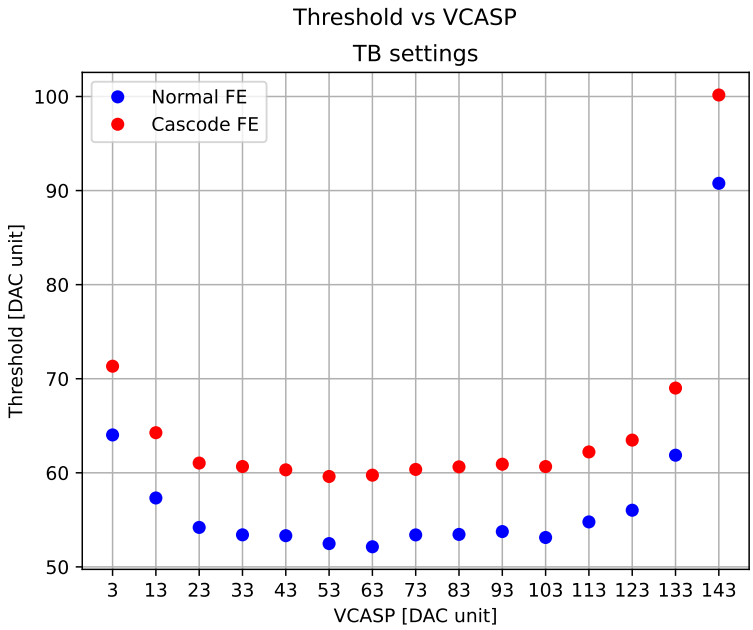

Figure 5.5: Trends of Threshold increasing V_{CASP}.

5.1.3.4 Time over Threshold (ToT)

The last analysis done in order to make a comparison with the simulations, is about the trend of the ToT changing the value of I_{CASN} for a fixed value of I_{THR} and vice versa. In particular we consider the data obtained with I_{CASN} fixed to 0 DAC and I_{THR} to 64 DAC, which are the values studied and used for this registers during the Test Beam in Desy.

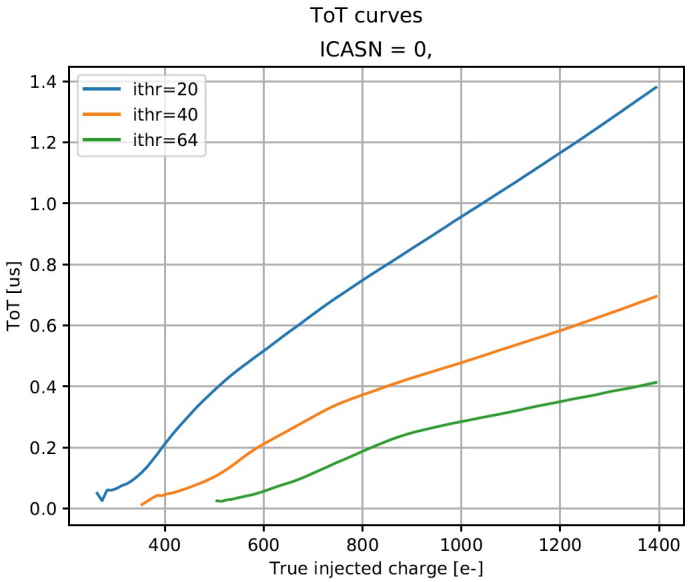

(a) ToT vs I_{THR} (I_{CASN}=0 DAC) - Data (**Cascode**)

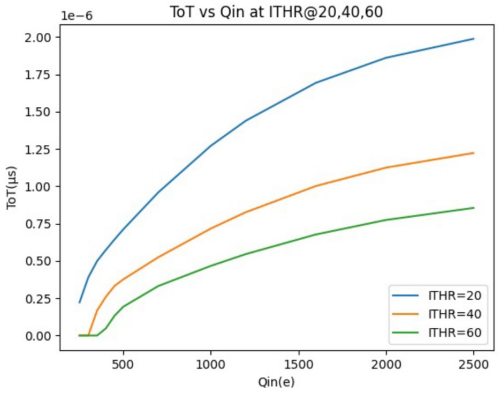

(b) ToT vs I_{THR} (I_{CASN}=0 DAC) - Simulation

Figure 5.6: ToT vs I_{THR}

In the last plots of this section (on page 30) are reported the trends of the ToT varying the value of V_{CASP} for both Normal and Cascode FE, but there aren't simulations to make a comparison.

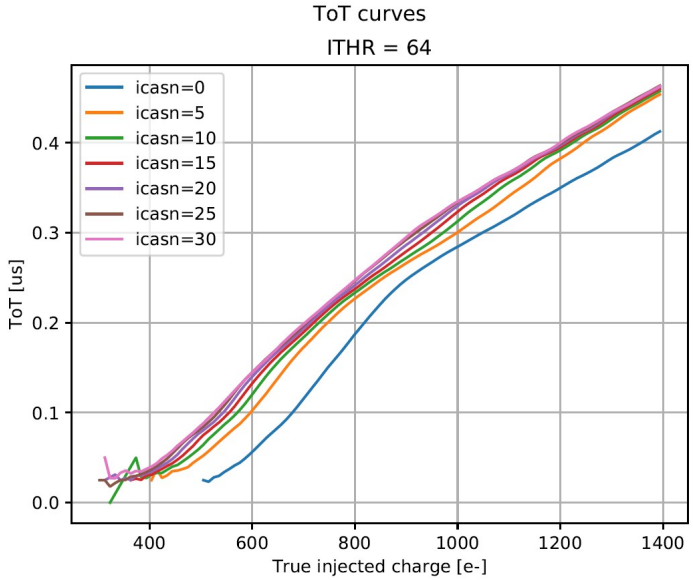

(a) ToT vs I_{CASN} (I_{THR}=64 DAC) - Data (**Cascode**)

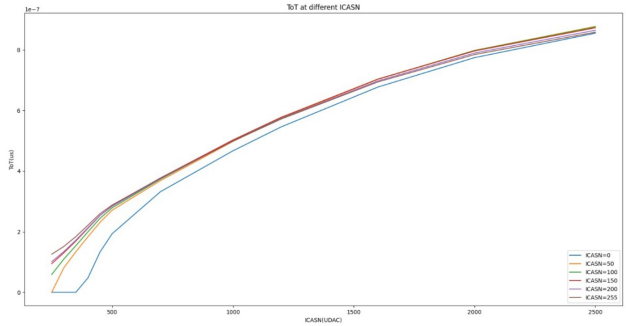

(b) ToT vs I_{CASN} (I_{THR}=64 DAC) - Simulation

Figure 5.7: ToT vs I_{CASN}

5.2 Characterization by injection

The ultimate purpose of this measurement is to describe (characterize) the response of each pixel by injecting a charge equivalent to the typical energy released from particles emitted in decays of radioactive materials. As explained in the previous section (reference), for example the ^{55}Fe has an emission spectrum with quite sharp lines and this allows to compare data more easily. The first line is at 5.9 KeV which corresponds on average to about 1616 e^- released (through the pixel??). For this reason it's mandatory to know the conversion between DAC and e^- [reference?] and to inject charges in order to study the pixel behaviour in the right regions, so those which are more interesting from a physical point of view.

Preliminarly it was necessary to study the threshold distribution on the whole matrix. The four flavors have been separately analyzed to be able to

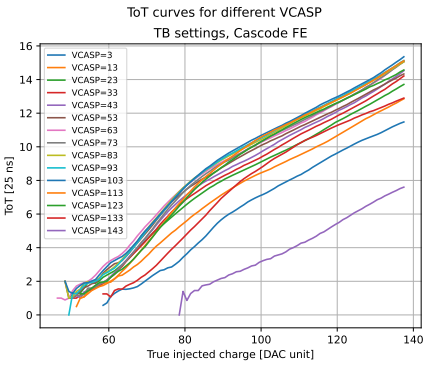

(a) ToT vs V_{CASP} - Data (**Cascode**)

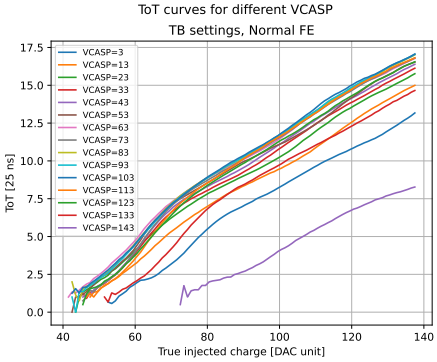

(b) ToT vs V_{CASP} - Data (**Normal**)

Figure 5.8: ToT vs V_{CASP}

study their main difference concerning their performance and features.

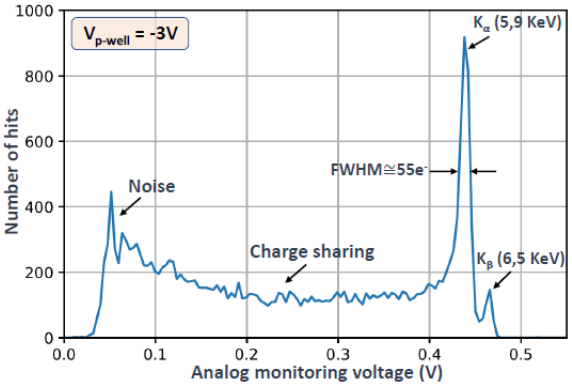

Figure 5.9: ^{55}Fe (radiactive source) emission spectrum using the analog output of a PMOS reset front-end of TJ-Monopix 1. (reference)

5.2.1 Injection circuit issues

In carrying out the measurements mentioned above, we started to noticed some issues with the injection circuit, which seemed to limit its working range. As a matter of fact the height of the injection pulse is expected to grow linearly increasing the value of charge to be injected. It actually happened up to a value of (about) $\approx$ 140 DAC, but for higher quantities of injected charge, the circuit seemed to increase not only the height of the signal, but also the threshold by a certain amount of ΔV (or equivalently of ΔQ, related by the conversion factor reported in REFERENCE). Moreover, for injection height grater than 200 DAC, only the threshold grows, without increasing the actual injected charge in any way.
We come to the conclusion that the grows of the threshold was artificial and due to the failure of the injection circuit.[?]

However as we have seen in the previous section (reference), the threshold depends on the settings of the chip registers and it can't be influenced by the injected charge, otherwise the whole response of the chip would be chaotic and it would not be reliable to take precise measurement of the impinging particles.

For this problem, the investigation on the behaviour of the threshold and its dispersion of all flavours of the matrix, required a series of additional measurements.
In the following sections the method used to obtain a reliable value of threshold and ToT is explained.

5.2.2 Measurement of the average threshold shift for injected charge greater than 140 DAC

To evaluate this artificial shift of the threshold, two different measurements have been done for each flavor:

- for an injected charge equal to 140 DAC $\rightarrow$ before the saturation region;
- for an injected charge equal to 200 DAC $\rightarrow$ almost the maximum limit of the saturation region (from this value onward only the threshold increases, not the injected charge).

The threshold distributions obtained from each measurements have been fitted to extract an average value on the whole flavor. Naming $Q_{th,140}$ and $Q_{th,200}$ the threshold obtained from injections of 140 and 200 DAC respectively, the mean shift has been estimated by:

$$\Delta Q = Q_{th,200} - Q_{th,140} \tag{5.1}$$

Eventually, this charge shift has been subtracted from data collected for an injection pulses of 200 DAC, in order to extrapolate the response in ToT of the injected pixels up to a value of 170 DAC.

What has been obtained is reported in the following section, together with a briefly explanation of the method used to evaluate the threshold.

5.2.3 Threshold and S-Curve

In order to obtain the thresold value for all pixels, each one of them has to be injected an arbitrary number of times (100 times in this work) for each value of the injection pulse between a minimum value, chosen setting the chip register "**VL**" and a maximum value set by the "**VH**" register, with a step of 1 DAC unit this is also adjustable).

So for each injection pulse height, the mean of 100 injection output are considered. In this way plotting the average number of detected hits in function of the injected charge, the typical curve better known as "*S-curve*" is reconstructed. It can be fit with the *error-function*,

$$errorfunc \tag{5.2}$$

from which the value of the threshold is evaluated considering the value of the injected charge at half of the curve's maximum height.

Specifically plotting the number of hits observed on each pixel divided by the total number of injections, for each injected charge, the half height corresponds to a charge value for which the pixel detects 50 hits of 100 injected and so when it has an occupancy of 0.5.

In the following are reported the results of this study for the flavors of all matrix.

5.2.3.1 Normal FE

The first flavor of the matrix is the **Normal FE**, which consist of 512 rows and 224 columns for a total of 114.688 pixels. In figure 5.10 on the next page are plotted all the s-curves of the all well-functioning Normal flavor pixels. The chip registers have been set with the same values used during the Test Beam at Desy (during...) which are reported in table 5.1.

Registri	Default Settings ("GOE")
ITHR	64
IBIAS	50
VRESET	143
ICASN	0
VCASP	93
VCASC	228
IDB	100
ITUNE	53
VCLIP	255
ICOMP	80
IDEL	88
IRAM	50

Table 5.1: Settings of the main registers used for the W14R12 chip, for Normal and Cascode flavors, during the Test Beam in Desy.

Using this setting, none of the pixels were noisy and so it wasn't necessary to use any mask.

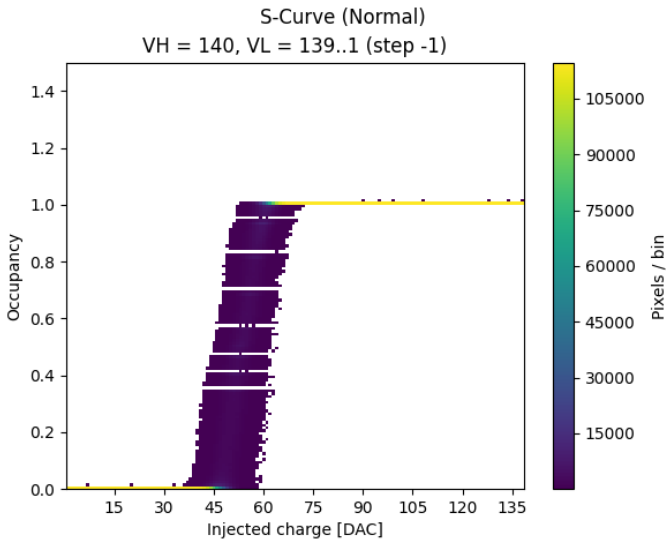

Figure 5.10: S-curves of all pixels of the Normal FE with an injection pulse of 140 DAC.

As already explained (in section...) the threshold distributions obtained from the two different measurements with an injection pulse of 140 and 200 DAC respectively, have been fitted and they are shown in figure 34 as representative examples also for the others flavors.

5.2.3.2 Cascode FE

Cascode FE is the second flavor and like **Normal FE** it consists of 512 rows and 224 columns for a number of total pixels equal to 114.688. For this flavor the same procedure of Normale FE has been followed and also the same values' registers (table 5.1 on the preceding page) have been used. There were not find noisy pixels. In figure **??** on page ?? the S-curves of all pixels are shown.

The fit of the threshold distributions instead, are shown in figure 5.13 on page 36.

5.2.3.3 HV-Cascode FE

The third flavor is **HV-Cascode FE** where HV stands for **High Voltage** and it is formed (counts) of 512 rows and 32 columns for a total number of pixel equal to 16384. Also for these last two flavors, the main chip registers are set with the same values tested and used during the Test Beam (@Desy) (but different from those used for the first two flavors). They are reported in table on page 35 .

As we can see from the plot of the alle S-curves in figure 5.14 on page 37, with these choices of values' registers, there were a lot of noisy pixels, but at this stage of measurements they were not masked. As a matter of fact along the y-axis of this plot is displayed the occupancy and when this values becomes higher than 1, it means that the pixel detects more hits than the injected ones, so it could be identified as "*noisy pixel*". [beacuse it results active regardless of

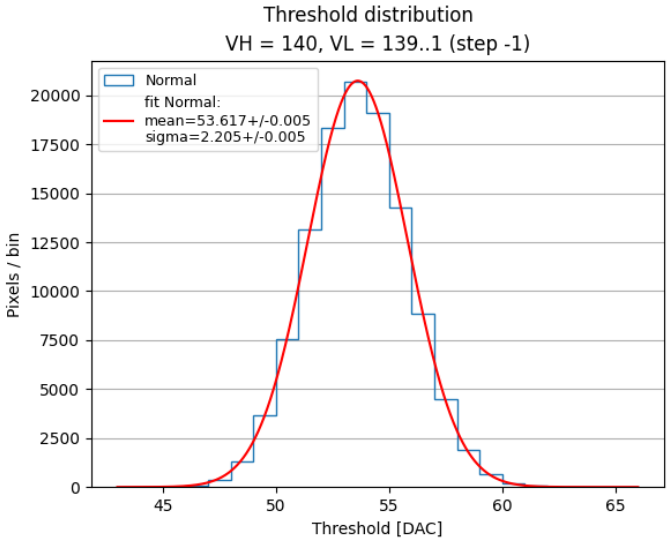

(a) VH = 140 DAC

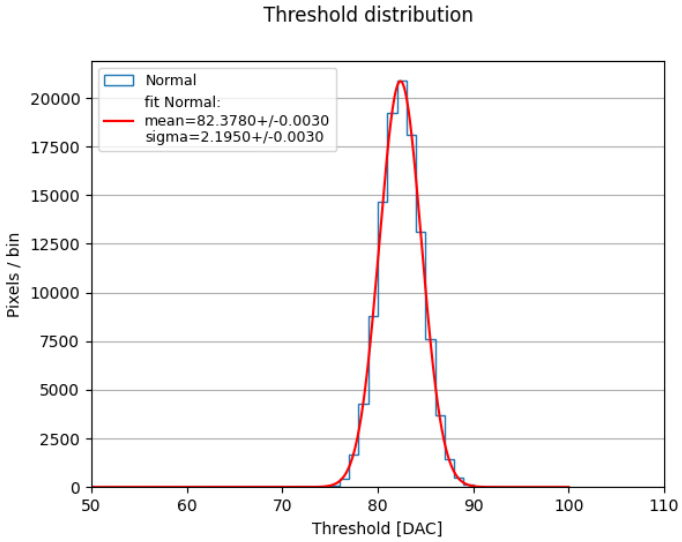

(b) VH = 200 DAC

Figure 5.11: Threshold distributions of **Normal** flavor before and at the maximum saturation, respectively.

the injection.]

In figure 5.17 on page 40 are shown the fit of the threshold distributions for the two different injections pulse.

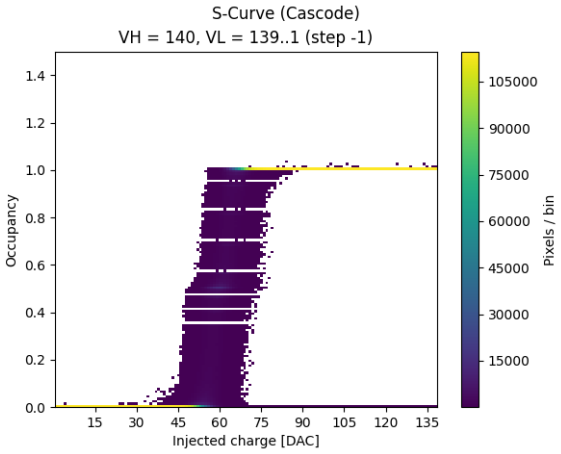

Figure 5.12: S-curves of all pixels in the **Cascode** flavor with an injection pulse of 140 DAC.

Registri	Default Settings ("GOE")
ITHR	30
IBIAS	60
VRESET	100
ICASN	8
VCASP	40
VCASC	228
IDB	100
ITUNE	53
VCLIP	255
ICOMP	80
IDEL	88
IRAM	50

Table 5.2: Settings of the main registers used for the W14R12 chip, for the HV's flavors, during the Test Beam in Desy.

5.2.3.4 HV-Normal FE

The fourth and last flavor is the **HV-Normal FE** which consists of 512 rows and 32 columns for a total number of pixel equal to 16.384. The main registers have been set with the values reported in table on the current page. In figure 5.16 on page 39, the S-curves of all pixel in the flavor. Also here we can see that there were some noisy pixels unmasked. Moreover, in this final flavor, the last 16 columns were not working and as a matter of fact they had return a peak of threshold near the value 0, which is excluded from the threshold distributions plots.

So actually in this part of the matrix, the real number of pixel studied was the half of the total, such as 8192 pixels.

In figure 5.17 on page 40 the fit of the threshold distributions for the two different values of injection height are reported.

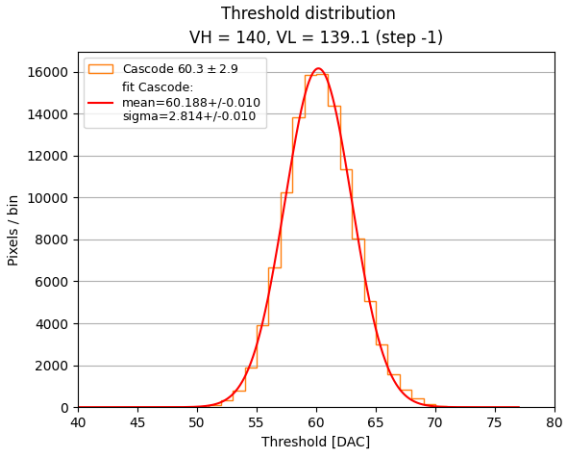

(a) VH = 140 DAC

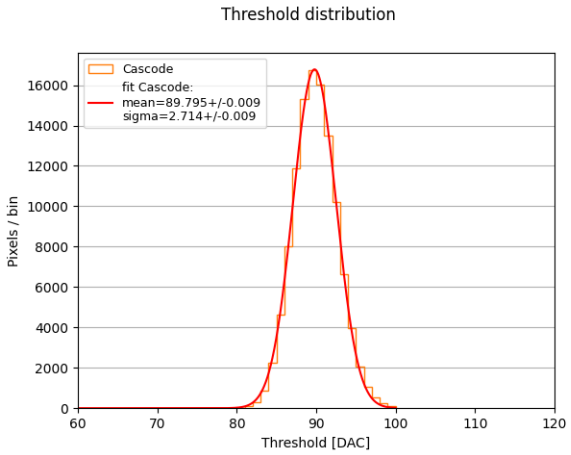

(b) VH = 200 DAC

Figure 5.13: Threshold distributions of **Cascode** flavor before and at the maximum saturation, respectively.

5.2.4 Noise and Equivalent Noise Charge (ENC)

5.2.5 Time Over Threshold (TOT) curves and fit

A side effect of the injection circuit issue is that the response of the chip can not be characterized in a region of charge that usually corresponds to the emission peaks of the radioactive sources available in the laboratory. For this reason, a fit of the ToT obtained at the maximum possible injected charge has been done, in order to extrapolate the most probable value of ToT in the main interesting region of charge.

The function chosen for this purpose is:

$$y(x) = a \cdot x + b - \frac{c}{x - t} \tag{5.3}$$

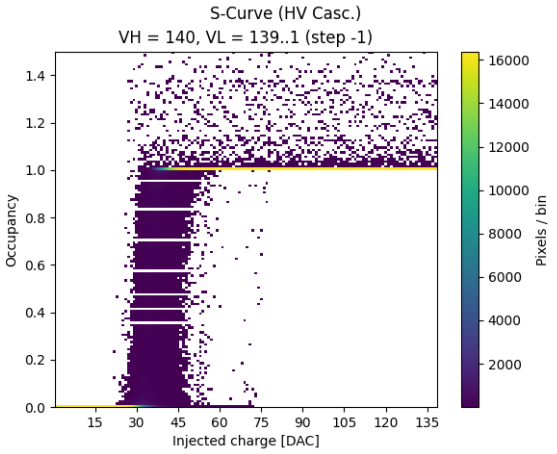

Figure 5.14: S-curves of all pixels in **HV Cascode** flavor with an injection pulse of 140 DAC.

with a, b, c and t free parameters.

Actually we know that the ToT distribution starts to grow near the threshold, so a random parameter could be computed in function of the threshold value estimated from the previous measurements, explained in section (reference).

In particular knowing that $y(x_{th})$ must be equal to 0, it can be imposed:

$$0 = a \cdot x_{th} + b - \frac{c}{x_{th} - t} \quad \Rightarrow \quad c = x_{th}^2 \cdot a + x_{th} \cdot (b - a \cdot t) - t \cdot b \qquad (5.4)$$

In this way the number of parameters to fit is reduced.

So the same data collected in the previous measurements of thresholds (for VH=200 DAC unit), have been used to fit the ToT curves of all pixels for each frontend. In table 5.3 are reported the value of the threshold considered for each frontend to extrapolate the value of the parameter $c$and the results of the fit for all parameters. In figure 5.18 on page 41 the results obtained for all Normal, Cascode and HVs FE.

	Normal	**Cascode**	**HV Cascode**	**HV**
threshold [DAC unit]	53.62	60.19	35.34	31.70
a				
b				
c				
t				

Table 5.3: Threshold and parameters obtained from the fit of ToT curve for each frontend.

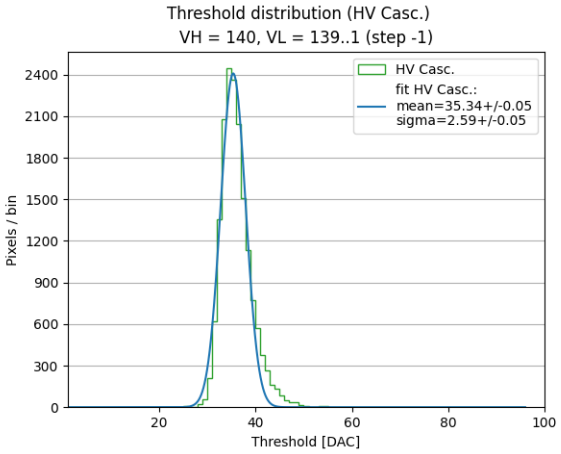

(a) VH = 140 DAC

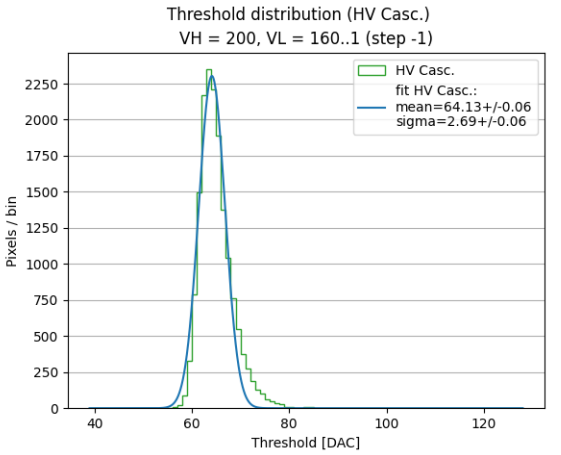

(b) VH = 200 DAC

Figure 5.15: Threshold distributions of **HV Cascode** flavor before and at the maximum saturation, respectively.

5.3 Radioactive sources

5.3.1 ^{55}Fe

CUT ON HVs flavors because of bad columns, many 0 ToT.

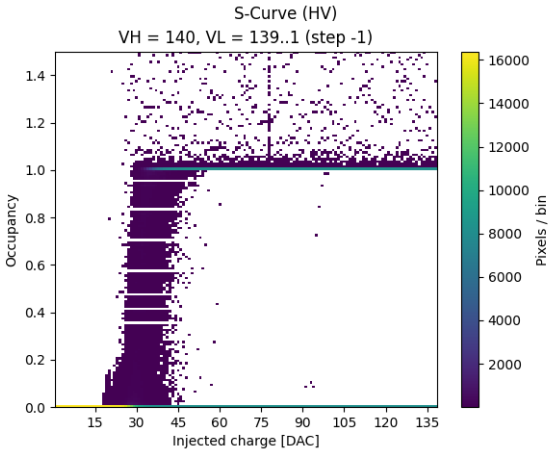

Figure 5.16: S-curves of all pixels in **HV Cascode FE** with an injection pulse of 140 DAC.

5.3.2 ^{241}Am

5.3.3 ^{109}Cd

5.3.4 ^{190}Sr

5.3.5 Injection capacitance calibration

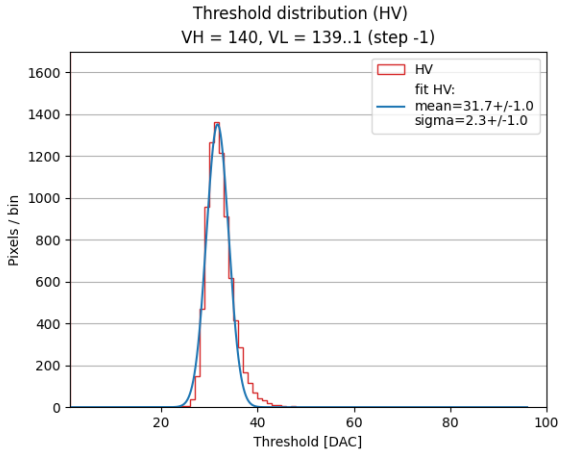

(a) VH = 140 DAC

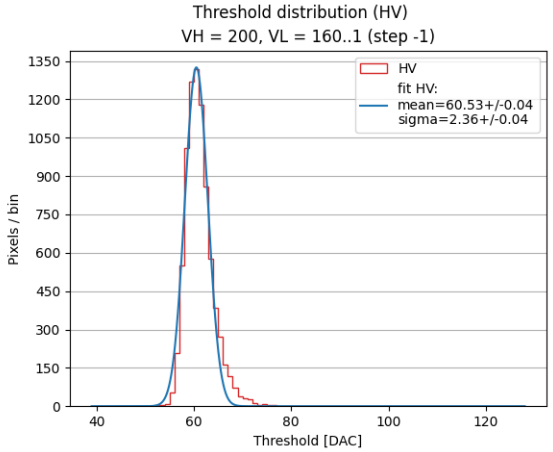

(b) VH = 200 DAC

Figure 5.17: Threshold distributions of **HV** flavor before and at the maximum saturation, respectively.

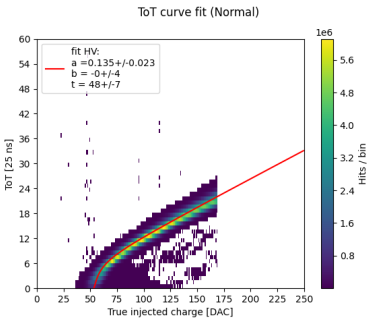

(a) **Normal**

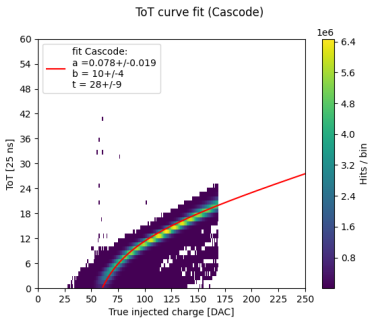

(b) **Cascode**

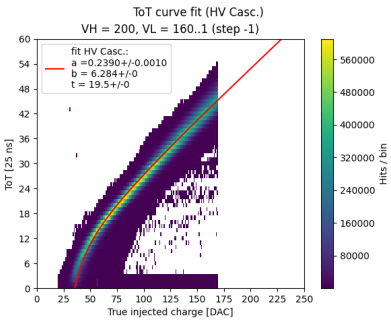

(c) **HV Cascode**

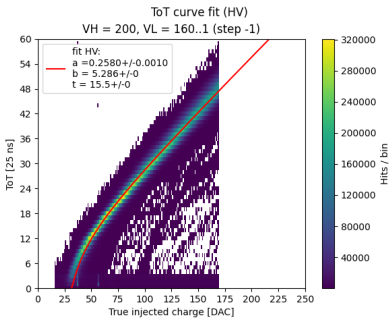

(d) **HV**

Figure 5.18: ToT curves fit for all frontend.

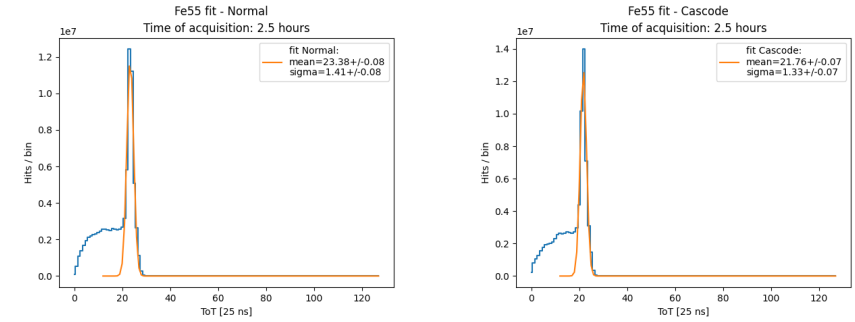

(a) **Normal** (b) **Cascode**

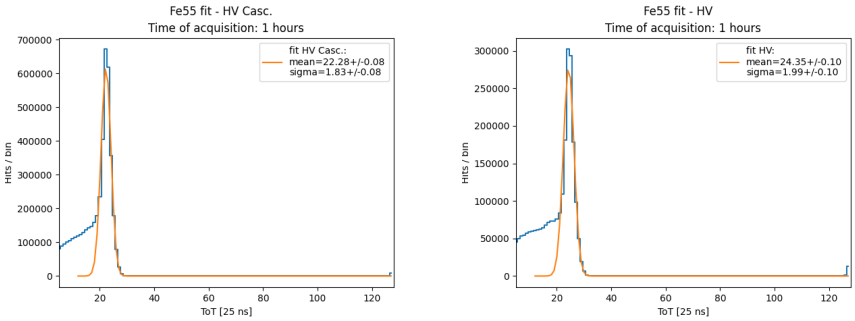

(c) **HV Cascode** (d) **HV**

Figure 5.19: ^{55}Fe pekas for all frontends.

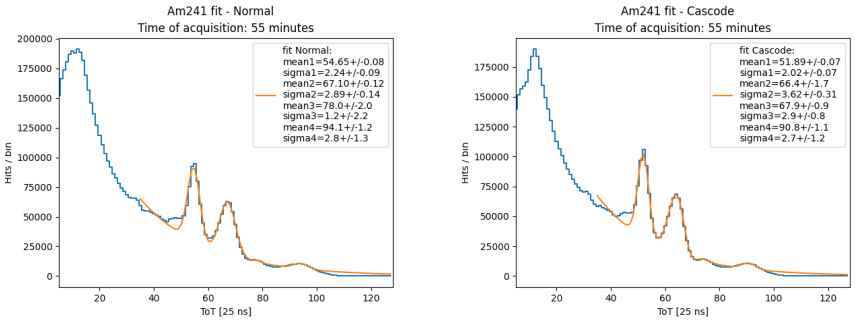

(a) **Normal** (b) **Cascode**

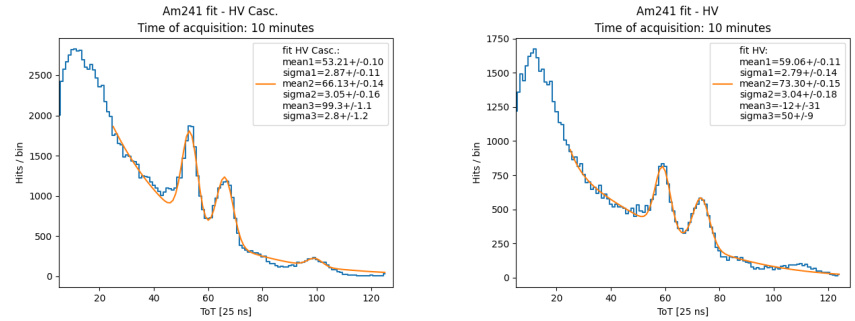

(c) **HV Cascode** (d) **HV**

Figure 5.20: ^{241}Am pekas for all frontends.

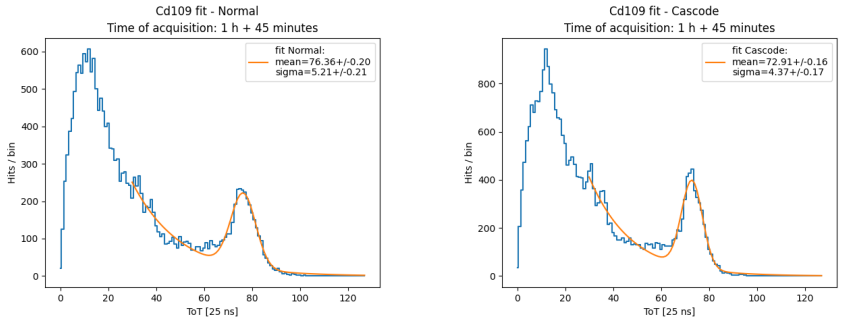

(a) **Normal**

(b) **Cascode**

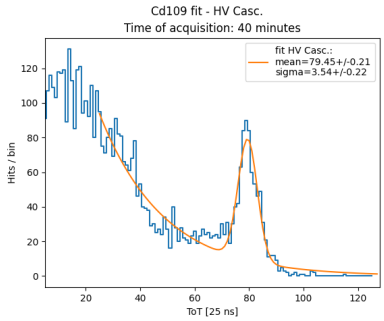

(c) **HV Cascode**

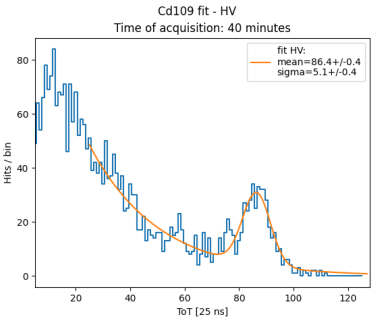

(d) **HV**

Figure 5.21: ^{109}Cd pekas for all frontends.

6. Conclusions